Microstructure and Mechanical Properties of Friction Stir Repaired Al–Cu Casting Alloy

Shude Ji[1] · Ruofei Huang[1] · Liguo Zhang[1] · Xiangchen Meng[1] · Zan Lv[1]

Abstract Friction stir repairing was successfully used to repair shrinkage cavity and porosity defects in Al–Cu casting alloy plates with T5 treatment. Effects of welding speeds on microstructures and mechanical properties of repaired region were mainly discussed. The results show that heat affected zone has the minimum microhardness due to coarser grains, where the tensile fracture is located. Through the thickness of the stir zone (SZ), the grain size decreases with increasing distance from the top surface of the repaired region due to the difference of heat input and cooling rate. The tensile strength and elongation of the SZ characterized by finer grains are both higher than those of the repaired region. These values of the SZ at 900 rpm and 150 mm/min reach 336.8 MPa and 11.75%, equivalent to 90.7 and 81.6% of BM without casting defects, respectively.

1 Introduction

With favorable mechanical properties at room and high temperatures, Al–Cu casting alloy has good potential for application in the aerospace field [1]. However, the poor castability of Al–Cu alloy, caused by a wide freezing range, is a difficult problem to be solved [2]. The wider freezing range always causes more porosity defects in a solidified aluminum casting structure [2]. The defects in casting alloy are detrimental to mechanical properties [3, 4]. Moreover, when the casting alloy structure is mechanically processed or is practically used, acceptably-small defects may change into unacceptably-large defects. Hence, weld-repairing is occasionally a necessary process for aluminum casting structures to save the production cost or operation cost.

Currently, fusion welding technologies have always been used for defect repair [5–11]. Li et al. [5] employed the gas tungsten arc welding (GTAW) to repair the porosity in cast D357 aluminum alloy and then improved the fatigue strength. Shankar et al. [6] used the tungsten inert gas (TIG) weld-repairing process to prevent the crack propagation of aluminum alloy 5083 plates and found out that weld-repairing process significantly increased the grain size in the heat-affected zone (HAZ) due to high heat input. Using the laser direct metal deposition, Pinkerton et al. [7] repaired H13 hot-work tool steel components and stated that porosity defects were unavoidable on the boundaries between the base metal (BM) and the added material. Besides the above-mentioned fusion welding technologies, other methods such as plasma transferred arc welding, HVOF thermal spraying and electron beam freeform fabrication can also be used to repair defects in metal structures [8–10].

Although some traditional fusion welding technologies can accomplish repair of defects in the metal structure, there are some shortcomings. In most cases, weld defects such as crack, inclusion and pore, may occur in the repaired region [11–14]. Although researchers have been paying more and more attentions on improving the weld-repairing process in the last several decades, few reports have focused on repairing

✉ Shude Ji
    superjsd@163.com

✉ Liguo Zhang
    zlgiast@163.com

[1] Faculty of Aerospace Engineering, Shenyang Aerospace University, Shenyang 110136, People's Republic of China

casting alloy by fusion welding, especially Al–Cu casting alloy due to high heat conductivity. In fact, as a solid state welding technique, friction stir welding (FSW) invented in the UK by TWI has the advantages of low distortion, no cracks, low power consumption and non-pollution [15, 16]. Therefore, FSW provides an effective way to repair casting alloy with high heat conductivity. Friction stir repairing (FSR), as a new variant of FSW, has attracted more and more attention at home and abroad. So far, some researchers, such as Liu et al. [17] and Jayaraman et al. [18], eliminated the original casting void defects by using the FSR. In this study, the FSR process has been utilized to repair shrinkage cavity and porosity defects in Al–Cu cast alloy plates. Meanwhile, microstructure, microhardness and tensile properties have mainly been discussed.

2 Experimental Procedure

In this study, the Al–Cu casting aluminum alloy plate, which was subjected to T5 treatment, was chosen as the BM. Its thickness, width and length were 10, 150 and 200 mm, respectively. The chemical compositions of the BM are listed in Table 1. X-ray non-destructive testing was used to find the region with casting defects in the Al–Cu casting alloy plates before repairing. Prior to the FSR, the surface of the region with casting defects was polished with an emery paper in order to remove the oxide layer.

FSR experiments with a tool tilt angle of 2.5° were performed using FSW machine (FSW-3LM-4012). H13 tool steel was used to fabricate the rotating tool. Figure 1 shows the schematic of the tool. In this study, the shoulder with concentric-circle flutes and the pin with right screw were designed to attain sufficient material flow [19]. The diameters of the shoulder, the pin tip and the pin bottom were 14, 5 and 3 mm, respectively. The pin length was 3.8 mm. Our previous experiments presented that a groove defect occurred in the weld when the rotating speed was lower than 900 rpm, resulting from low heat input and insufficient material flow, as displayed in Fig. 2. Therefore, the rotating speed of 900 rpm was chosen in this study. The welding speeds were respectively 100, 150 and 200 mm/min. Moreover, a plunge depth of 0.1 mm was chosen in order to realize a small thickness reduction.

X-ray radiographic inspection was performed on the repaired region. In this study, the region below the pin
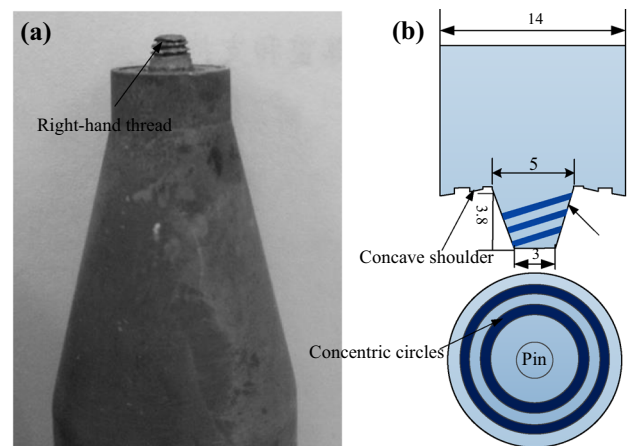

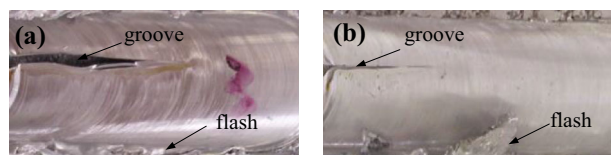Fig. 1 a Rotating tool used in experiment and b its dimensions (mm)

Fig. 2 Top surfaces of repaired region under a 700 rpm and 100 mm/min and b 800 rpm and 100 mm/min

along plate thickness was removed by means of milling in order to discuss the tensile properties of the repaired region. According to weld region tensile test standard ISO 4136: 2012, tensile samples were machined by wire electrical discharge machining, as shown in Fig. 3. Moreover, the tensile samples with small dimensions were also investigated to evaluate the tensile properties of stir zone (SZ). Tensile tests with a stretching speed of 2 mm/min were conducted on an electro mechanical controlled universal testing machine (RG4300). The average values of tensile specimens were presented for discussion. Specimens were cut from the FSR plates to carry out microstructure and microhardness characterization. A Vickers microhardness tester (HVS-1000) was used to measure the hardness. The testing step, testing force and dwell time were 0.5 mm, 100 g and 10 s, respectively. The microstructure specimens were prepared according to the standard procedures including grinding, polishing and etching. The specimens were etched with a reagent (1 ml hydrofluoric acid, 1.5 ml hydrochloric acid, 2.5 ml nitric acid and 95 ml water) to observe the microstructures of the repaired region. The microstructure and macrostructure

Table 1 Chemical compositions of material

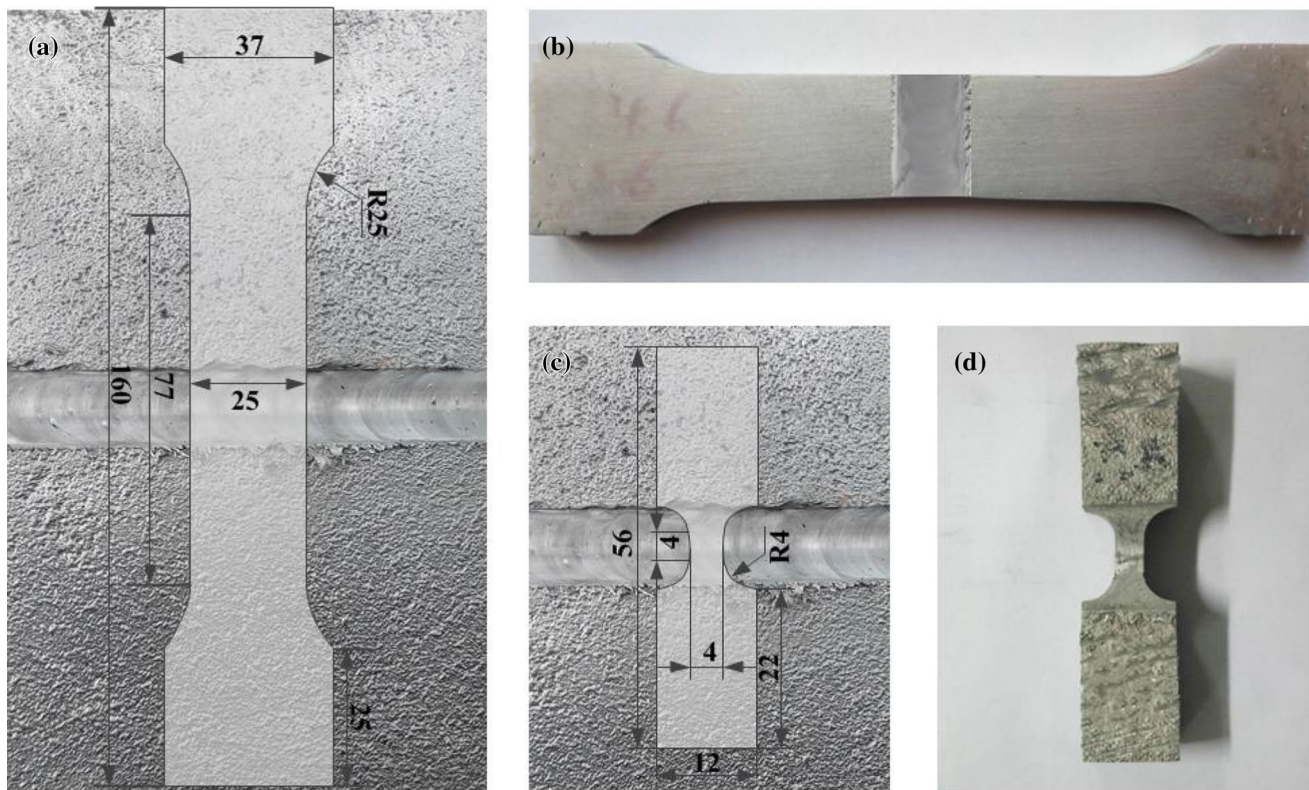| Element	Cu	Ma	Ti	Cd	Al
Specification	4.5–5.1	0.35–0.8	0.15–0.35	0.07–0.25	Balance

Fig. 3 Schematic diagrams of **a** repaired region (mm) and **c** SZ (mm); tensile samples of **b** repaired region and **d** SZ

were analyzed using an optical microscope (OLYMPUS, GX71).

3 Results and Discussion

3.1 Surface Formation

The liquid metal flows into the casting mould during the casting process, and then the casting structure can be obtained after the solidification of metal. For any casting technique, casting defects are unavoidable. Figure 4 presents the shrinkage cavity and porosity in the Al–Cu alloy plate and Fig. 5a displays the X-ray non-destructive test

photo of casting alloy plate before repairing. As reported by Mo et al. [4], a shrinkage cavity larger than 80 μm greatly influences the fatigue properties of casting structure. In Fig. 4a, the diameter of shrinkage cavity is more than 200 μm, so this defect need be repaired. In fact, besides the groove defect in Fig. 2, other volume defects of cavity and tunnel possibly occur in the SZ only when the material flow is insufficient during the repairing process. Therefore, X-ray non-destructive test is performed after repairing in order to know whether the volume defects induced by the FSR have been formed in the SZ. Figure 5b is the X-ray non-destructive test photo of the repaired region at 200 mm/min. It is concluded that the shrinkage cavity and porosity defects can be successfully repaired by FSR without extra material

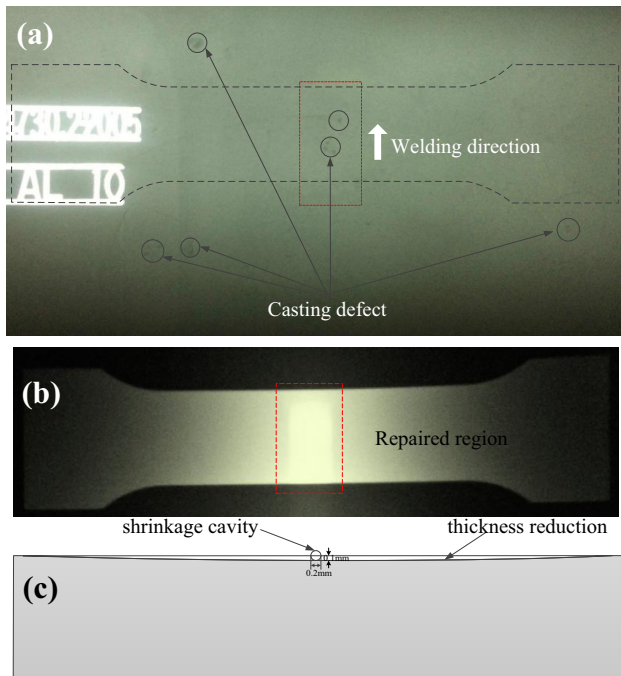**Fig. 4** Defects of Al–Cu alloy BM
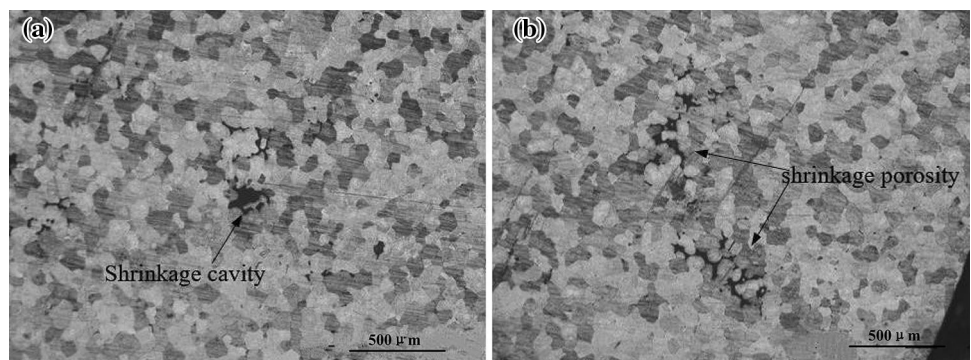
Fig. 5 X-ray non-destructive photos of **a** casting alloy plate before repairing and **b** repaired region at 200 mm/min; **c** schematic of area difference between shrinkage cavity and thickness reduction

addition into the BM. Although the diameter of shrinkage cavity (200 μm) in Fig. 4a is larger than the plunge depth of the tool (100 μm), the cross section of plate thickness reduction induced by the tool possesses a much larger area than that of shrinkage cavity, as presented in Fig. 5c. This is the reason why the casting defects in Fig. 4 can be repaired by the FSR process when an extra material is not used. Certainly, an extra material is necessary to endure the quality of repairing process when the volume of plate thickness reduction is smaller than that of casting defects, which has not been discussed in this study.

The surface formations of FSR regions are presented in Fig. 6. Similar to FSW joint [20], the shoulder marks and the flashes are also the typical features on the top surface of the repaired region. During the FSR process, the tool not only rotates but also moves along the designed path. These movement characteristics lead to the occurrence of the
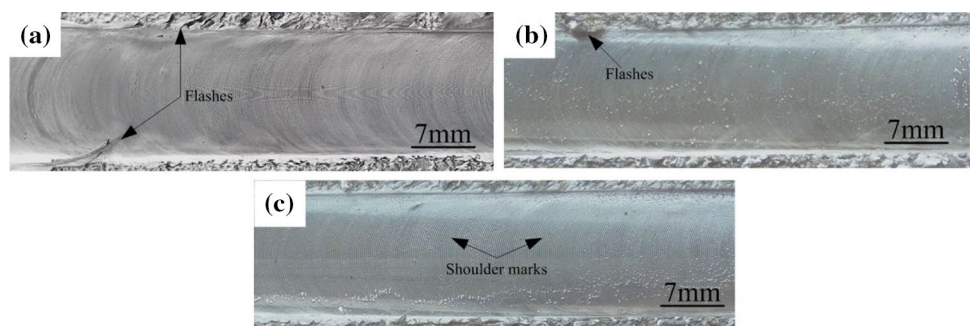
shoulder marks. Generally speaking, the distance between the shoulder marks is proportional to the ratio of welding speed to rotating speed. At the low welding speed of 100 mm/min, the adjacent two shoulder marks can be difficultly distinguished (Fig. 6a). The distance between the shoulder marks increases with increasing the welding speed, and its value is approximately 0.2 mm at 200 mm/min (Fig. 6c). Moreover, some plasticized materials with high temperature are squeezed out of the repaired region, and then the flashes are formed (Fig. 6). Due to the small plunging depth of 0.1 mm, the flashes in Fig. 6 are relatively small.

3.2 Macrostructure and Microstructure

The cross sectional morphology of the repaired region at 200 mm/min is shown in Fig. 7. It is seen that the defect-free SZ is attained. The tool used in this study consists of the shoulder with a large diameter and the pin with a small diameter, leading to the bowl-like morphology of the SZ. According to the morphology of cross section, the SZ can be divided into the shoulder affected zone (SAZ) and the pin affected zone (PAZ). In the PAZ, onion ring can be observed, presenting sufficient material flow behavior during the FSR process. Similar to traditional FSW, thermo-mechanically affected zone (TMAZ) and HAZ are also found, as shown in Fig. 7. In view of the change of microstructure and mechanical properties, the combination of the SZ, the TMAZ and the HAZ is named as the repaired region in this study. Due to the difference in force direction, the interface between the TMAZ and the SZ at the advancing side (AS) is much clearer than that at the retreating side (RS), which is similar to the experimental results reported by Liu et al. [21].

The recrystallization phenomenon induced by high temperature occurs in the SZ during the FSR process. Moreover, the material in the SZ undergoes violent flow resulting from the tool rotation with a high rotating speed. Therefore, the dynamic recrystallization (DRX) occurs [22, 23]. Similar to traditional FSW [24], the SZ of the repaired region is featured with fine and equiaxed grains, as
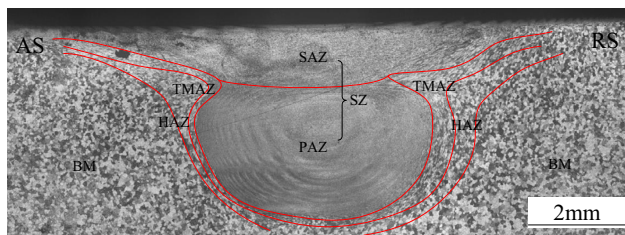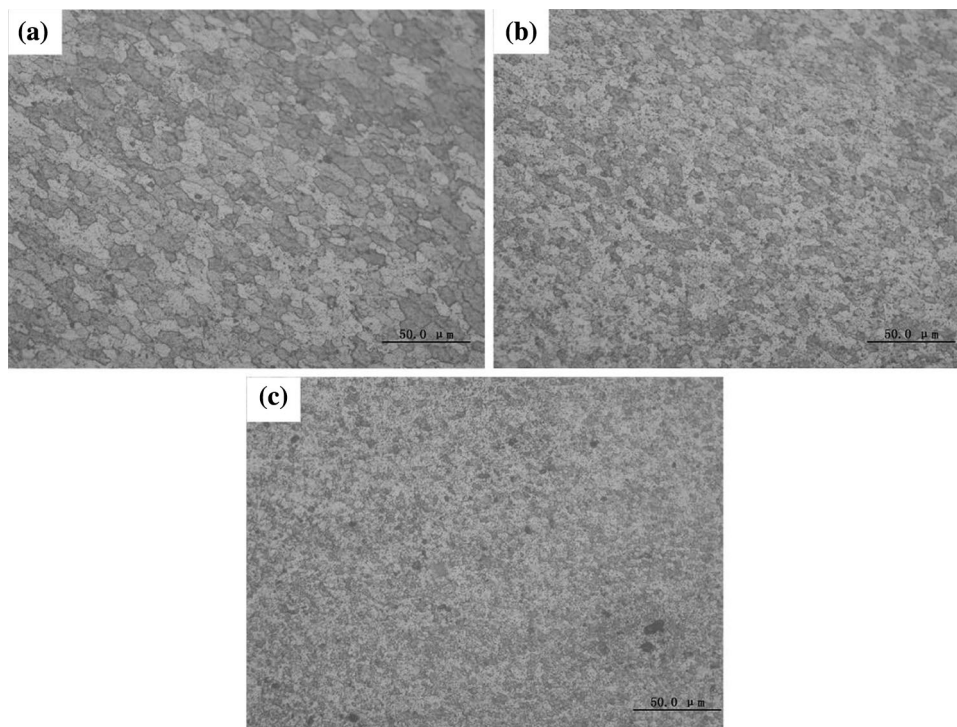
Fig. 6 Surface formations of repaired regions under different welding speeds: **a** 100 mm/min, **b** 150 mm/min and **c** 200 mm/min

Fig. 7 Cross section of repaired region at 200 mm/min

displayed in Fig. 8. Frictional heat generated by the tool can be divided into two parts during the FSR process. One is the heat by the shoulder, the other is the heat by the tool pin. Because of the difference in tool diameter and force, the heat generated by the shoulder is much more than that by the pin. In this study, the pin with the length of 3.8 mm has been used to repair the casting alloy plate with the thickness of 10 mm. Therefore, compared to the SZ center and top, much more frictional heat in the SZ bottom is more easily transferred towards the region below the pin. This condition easily results in a large temperature gradient along the plate thickness during the FSR process, leading to the difference in grain size between the different regions of SZ. Zhang et al. [25] reported that increasing backplate diffusivity was beneficial in attaining the SZ with finer grains, which results from the same reason as the experimental results in this study. The average grain size of the SAZ in Fig. 8a is 10.6 μm and its value is larger than that (9.8 μm) of the PAZ top in Fig. 8b. The grain size of the

PAZ bottom (Fig. 8c) is the smallest and its value is 7.2 μm.

Figure 9 shows the microstructures in the TMAZ along the repaired region thickness. During the FSR process, the material in the TMAZ undergoes a moderate deformation and relatively lower temperature compared to the SZ, leading to the elongated grains. As mentioned above, the temperature in the SAZ is higher than that in the PAZ, which results in bigger grains in the top region in the TMAZ (Fig. 9a) compared with middle or bottom region (Fig. 9c, e). The plunging of the tool shoulder makes the material in the TMAZ flow downwards (Fig. 9a, b). The material in the PAZ flows downwards with the rotation of tool pin and then accumulates near the pin tip. The accumulated material near the pin tip pushes the material in the TMAZ to transfer upwards according to the minimum resistance law (Fig. 9c–f). Moreover, the elongated extent of grain in the TMAZ decreases with the increase in distance from the SZ, which is mainly related to the material flow behavior and the temperature distribution during the FSR process. In addition, it is further attained that the boundary between the SZ and the TMAZ at the AS is more easily distinguished than that at the RS.

Moreover, the microstructures in the PAZ under different welding speeds are compared, as presented in Fig. 10. Generally speaking, increasing welding speed can reduce heat input per unit length, resulting in the decrease of welding peak temperature. The lower the peak temperature is, the shorter the growth time of grain in the SZ. The

Fig. 8 Microstructures along the thickness of SZ at 200 mm/min: **a** SAZ, **b** PAZ top and **c** PAZ bottom

Fig. 9 Microstructures of TMAZ at 200 mm/min: top regions at **a** AS and **b** RS, middle regions at **c** AS and **d** RS, bottom regions at **e** AS and **f** RS
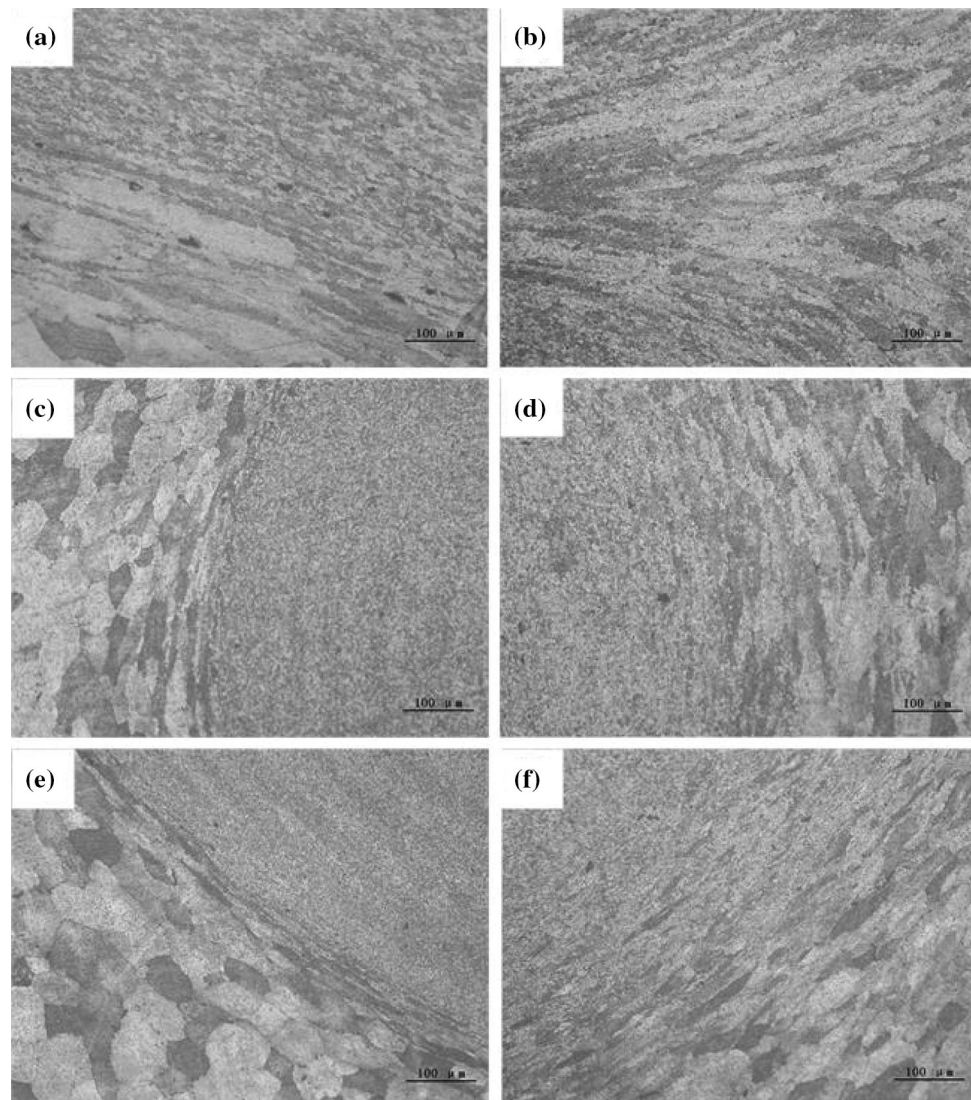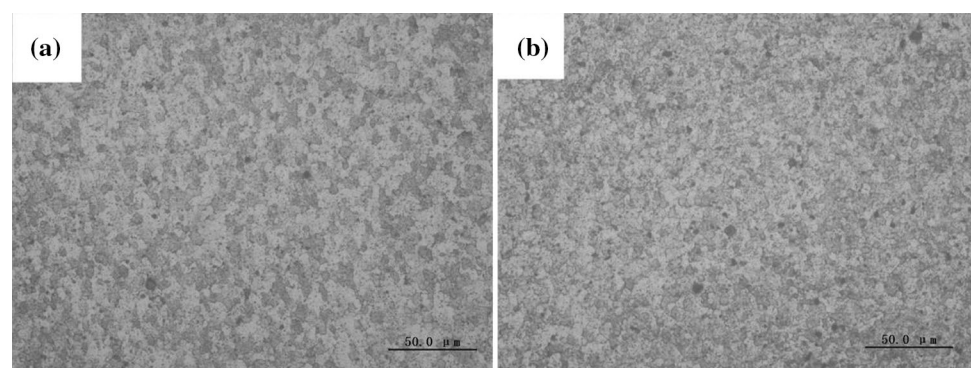

Fig. 10 Microstructures at PAZ bottom under different welding speeds: **a** 100 mm/min and **b** 150 mm/min

grain size of 8.11 μm at 150 mm/min in Fig. 10b is larger than that at 200 mm/min in Fig. 8c. The grain size at 100 mm/min is the biggest and its value is 9.12 μm, as presented in Fig. 10a.

3.3 Mechanical Properties

3.3.1 Microhardness

As schematically shown in Fig. 11, two test lines are measured. Thereinto, one test line perpendicular to the
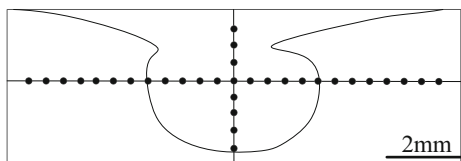
Fig. 11 Schematic illustration of the FSR region for microhardness tests

plate top surface is located at the center of SZ. Measured points of the other test line are all 2 mm away from the plate top surface. Figure 12 presents the microhardness of the repaired region. It is seen that the microhardness distribution presents a W shape (Fig. 12a). The BM microhardness is approximately 110Hv. In this study, Al–Cu alloy with T5 treatment is a kind of precipitate strengthening alloy. Therefore, the BM in Fig. 9 has the highest microhardness since the SZ, the TMAZ and the HAZ all undergo a high enough temperature. The HAZ with coarser grains possesses the lowest microhardness. Its minimum value is 89.8Hv, which is located at the HAZ adjacent to the TMAZ at the RS. According to the Hall–Petch relation, the finer grains are beneficial in increasing the hardness of the material [26]. Therefore, the microhardness of the SZ with smaller grains is higher than that of the HAZ. Moreover, the microhardness along the SZ thickness mainly increases with the increase of distance from the top surface of repaired region (Fig. 12b), resulting from the difference in grain size. In Fig. 12b, the hardness with the distance of 0.5 mm from the top surface is relatively higher, which may result from a higher cooling rate compared with the other regions in the SAZ and the PAZ top.

3.3.2 Tensile Properties

Tensile tests of repaired regions have been performed and the results are shown in Fig. 13. Due to the minimum microhardness, the HAZ of the repaired region always is the weakest region, where the fracture position is located. Figure 14 indicates the fracture locations of tensile specimens of the BM without casting defects and the repaired regions. In this study, the tensile strength and elongation of the BM without casting defects are respectively 371.2 MPa and 14.4%. From engineering stress and strain diagrams in Fig. 13a, it is known that all tensile specimens present a good ductile property because the tensile strength is much higher than the yielding strength at the same welding parameters. With increasing welding speed from 100 mm/min to 200 mm/min, the tensile strength and elongation of the repaired region both increases and then decreases. At 150 mm/min, the tensile strength and elongation of the repaired region reach the maximum values of 301.6 MPa and 11.06%, equivalent to 81.3 and 76.8% of the BM without casting defects, respectively. Figure 15 indicates the tensile properties of the SZ. As mentioned above in Figs. 8c and 10, the SZ is composed of fine and equiaxed grains, leading to higher tensile properties than the HAZ. Therefore, the SZ easily possesses better tensile properties than the repaired region. When the welding speed increases from 100 mm/min to 150 mm/min, the tensile properties of the SZ increases due to the finer DRX grains. When the welding speed further increases to 200 mm/min, the tensile properties reduces, which may result from a higher heat input compared to 150 mm/min. The tensile strength and elongation of the SZ at 150 mm/min reaches 336.8 MPa and 11.75%, equivalent to 111.7 and 106.2% of the repaired region.

Figure 16 exhibits the fracture surface morphologies of the SZs under different welding speeds. It is seen that the fracture surfaces are both featured by dimples with various sizes and depths. At 100 mm/min in Fig. 16a, a part region of the fracture surface has nearly no dimples, which may result from a low bonding strength. Compared with the SZ
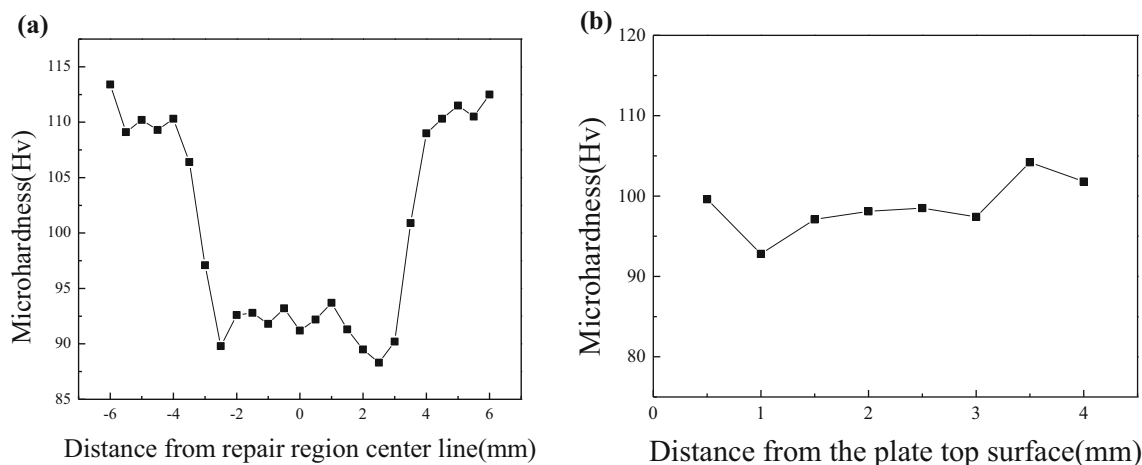

Fig. 12 Microhardness of repaired region at 200 mm/min: **a** across the cross section, **b** along the plate thickness
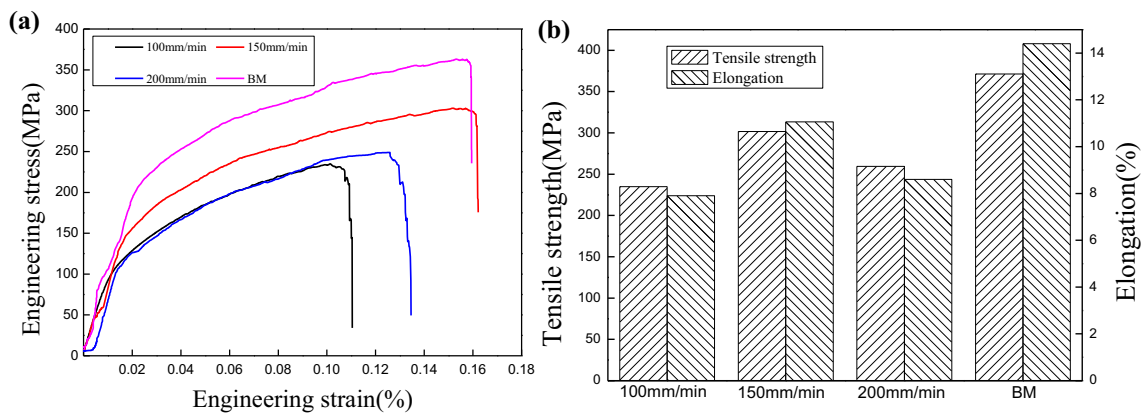
Fig. 13 Tensile properties of repaired regions under different welding speeds: **a** engineering stress and strain diagram and **b** tensile strength and elongation

Fig. 14 Fracture locations of tensile specimens

at 100 mm/min, the fracture surface at 150 mm/min possesses more, larger and deeper dimples. The morphology of dimples on the fracture surface is closely related to the ductility of material. The elongation of material increases with the improvement of ductility property. Therefore, the experimental results of fracture surface morphologies in Fig. 16 are in good agreement with the results in Fig. 15. Therefore, so long as the welding parameter's combinations, such as the rotating speed of 900 rpm and the welding speed of 150 mm/min, are reasonably chosen, the ductile fracture of SZ can be attained.

4 Conclusions

By choosing Al–Cu casting alloy plates with the thickness of 10 mm as research objects, FSR was successfully performed. Formation and mechanical properties of repaired region were mainly investigated. The following conclusions could be extracted.

(1) Shrinkage cavity or porosity casting defects can be successfully repaired by the FSR without an extra material addition into the BM. The repaired region consists of SZ with a bowl-like geometry, TMAZ with deformed and enlarged grains and HAZ with coarser grains.

(2) Due to the difference in heat input and heat loss, the fine and equiaxed grains in the SZ top and bottom are the largest and the smallest, respectively. Increasing the welding speed is beneficial in reducing the grain size in the SZ.

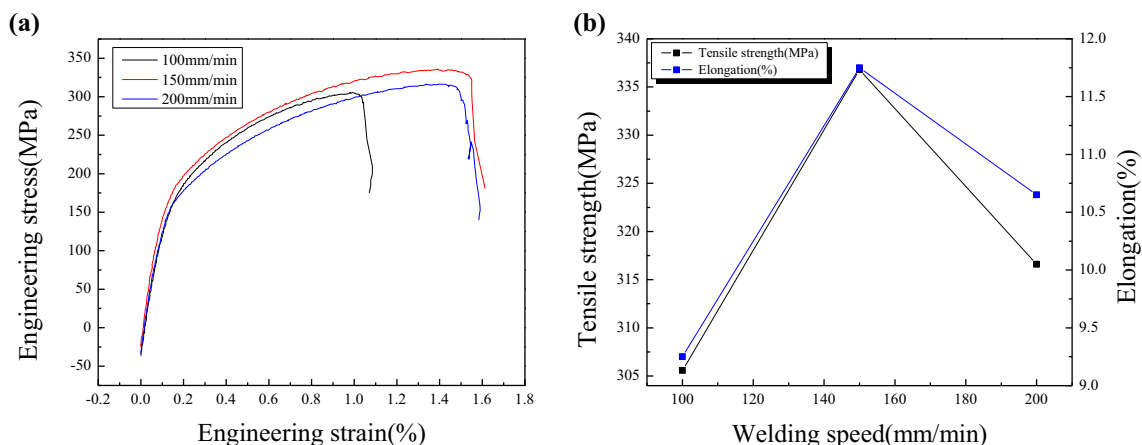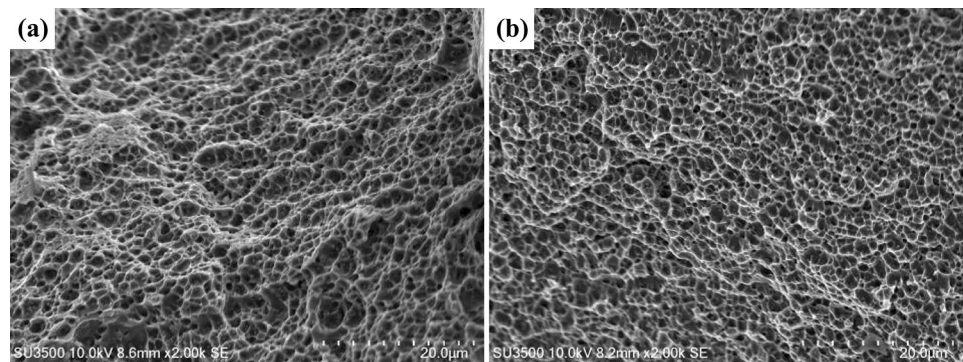(3) When the welding speed varies from 100 mm/min to 200 mm/min, the tensile properties of the repaired

Fig. 15 Tensile properties of SZs under different welding speeds: **a** engineering stress and strain diagram and **b** tensile strength and elongation

Fig. 16 Fracture surface morphologies of SZs under different welding speeds: **a** 100 mm/min and **b** 150 mm/min

region and the SZ both increase and then decrease due to the variation of heat input. At 150 mm/min, the tensile strength and elongation of the SZ reach 90.7 and 81.6% of the BM without casting defects, respectively. The SZ possesses higher tensile properties than the repaired region and its fracture surface morphology presents the ductile fracture.

References

1. Samal S, and Phanikumar G, *Trans Indian Inst Met* **68** (2015) 122.
2. Kuo Y S, PhD Thesis, National Cheng Kung University, Tainan, Taiwan, ROC (1990).
3. Ceschini L, Morri A, and Sambogna G. T, *J Mater Process Technol* **204** (2008) 231.
4. Mo D F, He G Q, Hu Z, and Zhang W H, *J Mater Eng* **7** (2010) 025.
5. Li L, and Snow M, *Weld J* **85** (2006) 264s.
6. Shankar K, and Wu W, *Mater Des* **23** (2002) 201.
7. Pinkerton A J, Wang W, and Li L, *Proc Inst Mech Eng B J Eng Manuf* **222** (2008) 827.
8. Su C Y, Chou C P, Wu B C, and Lih W C, *J Mater Eng Perform* **6** (1997) 619.
9. Tan J C, Looney L, and Hashmi M S J, *J Mater Process Technol* **92** (1999) 203.
10. Tu J F, and Paleocrassas A G, *J Mater Process Technol* **211** (2011) 95.
11. Xu W F, Liu J H, and Chen D L, *J Mater Sci Technol* **31** (2015) 953.
12. Yusof M F M, Kamaruzaman M A, Ishak M, and Ghazali M F, *Int J Adv Manuf Technol* (2016). https://doi.org/10.1007/s00170-016-9343-4.
13. Jayaraman M, Sivasubramanian R, and Balasubramanian V, *Trans Nonferrous Met Soc China* **23** (2013) 605.
14. Feng J, Guo W, Irvine N, and Li L, *Int J Adv Manuf Technol* (2016). https://doi.org/10.1007/s00170-016-8929-1.
15. Ji S D, Meng X C, Huang R F, Ma L, and Gao S S, *Mater Sci Eng A* **664** (2016) 94.
16. Huang Y X, Han B, Tian Y, Liu H J, Lv S X, Feng J C, Leng J S, and Li Y, *Sci Technol Weld Join* **16** (2013) 497.
17. Liu H J, Fujii H, and Nogi K, *Mater Sci Technol* **20** (2004) 399.
18. Jayaraman M, Sivasubramanian R, Balasubramanian V, and Lakshminarayanan A K, *J Sci Ind Res* **68** (2009) 36.
19. Gunter C, Miles M P, Liu F C, and Nelson T W, *J Mater Sci Technol* (2017). https://doi.org/10.1016/j.jmst.2017.10.023.
20. Ji S D, Meng X C, Liu Z L, Huang R F, and Li Z W, *Mater Lett* **201** (2017) 173.
21. Liu Z L, Cui H T, Ji S D, Xu M Q, and Meng X C, *J Mater Sci Technol* **32** (2016) 1372.
22. Navaser M, and Atapour M, *J Mater Sci Technol* **33** (2017) 155.
23. Zhang Z H, Li W Y, Feng Y, Li J L, and Chao Y J, *Acta Mater* **92** (2015) 117.
24. Fratini L, Buffa G, Palmeri D, Hua J, and Shivpuri R, *J Eng Mater Technol* **128** (2006) 428.
25. Zhang Z H, Li W Y, Shen J J, Chao Y J, Li J L, and Ma Y E, *Mater Des* **50** (2013) 551.
26. Ji S D, Meng X C, Zeng Y M, Ma L, and Gao S S, *Mater Des* **97** (2016) 175.